euspen's 20th International Conference & Exhibition, Geneva, CH, June 2020
www.euspen.eu

In-situ displacement measurement for use in LHC collimators

Tom Furness[1], James Williamson[1], Simon Fletcher[1], Ali Iqbal[1], Andrew Bell[1], Andrew Henning[1], Haydn Martin[1], Xiangqian Jiang[1], Alessandro Bertarelli[2], Federico Carra[2], Michele Pasquali[2], Stefano Radaelli[2]

[1]*The Univeristy of Huddersfield, Queensgate, Huddersfield, HD1 3DH, United Kingdom*
[2]*CERN, Espl. des Particules 1, 1211 Meyrin, Switzerland*

T.furness@hud.ac.uk, J.f.williamson@hud.ac.uk

Abstract

The Adaptive Collimation System (ACS) is a closed-loop control system that can monitor and correct collimator jaw straightness deviations. Key to the operation of the ACS is a fibre-based interferometric strain measurement system mounted in the jaws that can detect straightness deviations. This system utilises spectral interferometry to interrogate multiple strain sensitive intrinsic Fabry-Perot interferometer (IFPI) cavities that can detect localised thermal and vibratory deformations within the jaw structure and allow for their correction. This paper outlines the operation of the fibre-based measurement system, construction and integration challenges, both environmental and mechanical. Finally, preliminary experimental results are described which indicate the system is sufficiently sensitive to observe a second order response from a 1.5 µm first order displacement (bend) of the jaw.

Keywords: Collimator, LHC, Strain measurement, Interferometry

1. Introduction

1.1 *The Role of Collimation in the LHC*

Currently each beam in the LHC (Large Hadron Collider) has 362MJ of stored energy. At these energy levels, even a small loss can quench a superconductive magnet, or damage more sensitive areas of the accelerator complex [1]. After the HL-LHC upgrade (High Luminosity LHC upgrade), these energy levels are set to more than double, increasing to over 700MJ [2]. To ensure machine protection the LHC employs a multi-stage collimation system designed to clean the beam tails, and dispose of outlying particles in a controlled manner.

Whilst the overall collimation system consists of multiple individual collimators of differing design and function, the design architecture in general remains the same. The basic design of a single collimator consists of two jaws that straddle the beam, enclosed in a vacuum tank, connected to a drive system that can move the jaws in respect to the beam line. A cross section of a secondary collimator is shown in figure 1. The main component of these jaws is the absorption areas. These areas are located closest to the beam in order to intercept the beam halo.

1.2 *Losses and induced deformation*

Critical to the operation of the collimator is jaw straightness. For the collimator jaws used in this study the maximum allowable straightness deviation is ±100µm. Transverse deformations in the jaw structure can significantly affect the interaction of the jaw with the beam concerning cleaning efficiency, impedance on the beam, and deposited thermal loads [3]. Flatness of the absorption blocks, angular misalignment, mechanical tolerances, and thermal deformation can all contribute to transverse deformation of the jaws.

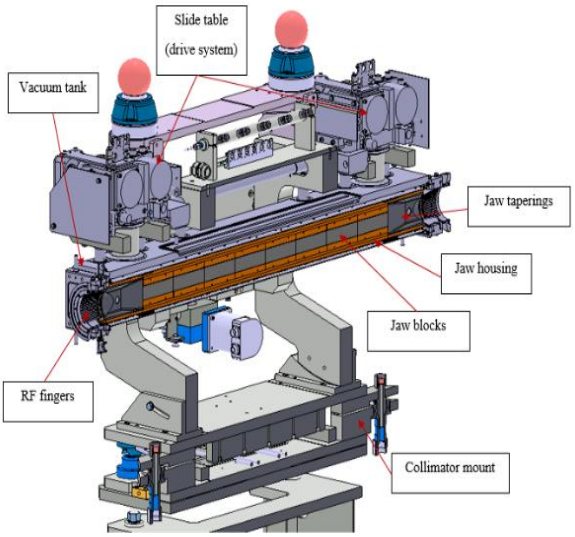

Figure 1. Cross Section of TCSPM Secondary Collimator

Most of the factors listed above can be mitigated using conventional methods. Jaw block flatness and mechanical tolerance can be limited in the assembly process and angular misalignment can be corrected to a certain degree by the collimator's drive system. However, thermal transverse deformations caused by energy depositions are much harder to detect and correct.

Whilst the collimator is performing its primary operation these thermal transverse deformations are inherent due to energy being deposited in the jaw from beam losses. To balance the thermodynamics of the system, the collimator jaws have a dedicated water fed cooling system. This cooling system is designed to evacuate the induced high heat loads whilst minimizing temperature gradients across the jaw [4].

For this design of collimator, a TCSPM secondary collimator, under steady-state operation the mechanical design of the

jaw and integrated cooling system can ensure that the thermal transverse deformations do not exceed the 100µm tolerance limit. However, several potential operational scenarios that can induce much larger deformations have been identified [5] [6]. High-energy quasi-static losses in the tens of kW range can cause elastic deformations with circa 0.5 mm magnitudes, whilst so-called "dynamic losses", such as injection errors or asynchronous beam dumps, can induce flexural vibratory responses with millimetre amplitudes, and result in plastic deformation.

1.3 *Adaptive collimation*

In an effort to resolve these thermally induced deformations, we have devised the Adaptive Collimation System (ACS). The ACS is a closed loop control system designed to monitor transverse deformations and where possible, correct for them ensuring that the front face of the collimator jaw remains within its straightness tolerance limit. Integrated into the design of a secondary TCSPM collimator, the ACS consists of a fibre based spectral interferometer to monitor the deformations, and a series of high-powered ceramic piezo-electric actuators to manipulate the jaw structure, in order to maintain its straightness. The scope of this paper will be focused on the aspects of the fibre based measurement system.

2. Spectral Interferometry for fibre strain measurement

At the inception of this project, it was envisaged that jaw monitoring would be performed by a custom designed slotted photo-microsensor based sensor. The original design of these sensors had a linear measurement range of 20 µm, with a resolution of 21 nm [7]. However, it was soon determined that these sensors would be unsuitable for this application due to lack of radiation tolerance. Twenty-eight of these sensors were exposed to a Cobalt 60 source for eight hours with a dose equivalent of 7439.3 mSv. After exposure, each sensor was tested for functionality, with only 12 of the original 27 operational. Given that LHC collimators are some of the more heavily irradiated components of the LHC a suitable alternative was needed.

With respect to this, a new strain measurement system using fibre optics and spectral interferometry has been designed and implemented, as commercially available systems do not meet the challenges of this application. It must be robust to electromagnetic radiation sources, as well as resistant to fibre darkening caused by ionising radiation. A long gauge length is desirable to achieve high strain resolution (<100 nε) and to achieve full spatial coverage of the collimator jaws (multiple strain sensors to measure first and second order shapes). A high measurement rate (>2000 Hz) is necessary to measure and quantify transient events while a low cost (<£10,000) is desirable to limit costs if this solution is accepted and scaled up to instrument future collimator designs.

2.1 Experimental Setup

Error! Reference source not found. shows a schematic of the optical setup. Light from a broadband ($\lambda_C = 850\ nm, \Delta\lambda$ =50 nm) superluminescent diode (SLED) enters a 2x2 fibre optic coupler (FOC) and then a 1x8 fibre switch (LightBend LBSW-1128120333) which allows selection of the active fibre strain gauge and hence time division multiplexing (TDM) of the strain signal. From the fibre switch, the source light travels along 5m lengths of single mode fibre (780 HP), through an 8x8 FC/APC vacuum port (not shown) into the collimator vacuum tank and along the collimator jaws to the fibre strain gauges (1 shown).

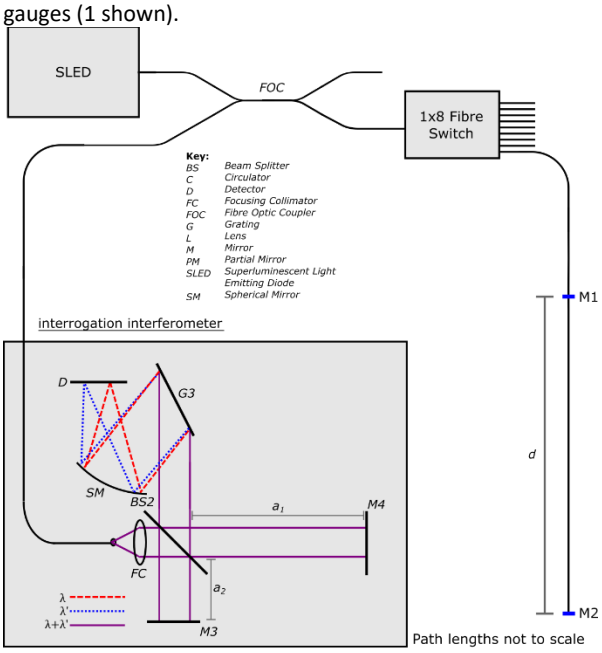

Figure 2. Schematic showing the optical layout of the strain sensitive intrinsic Fabry-Perot interferometer (IFPI) and remote interrogation interferometer.

Each of these strain sensitive regions comprises a cavity (intrinsic Fabry-Perot interferometer (IFPI)) formed by two reflective surfaces within the fibre, M1 and M2, separated by the gauge distance, d. Further details of the IFPI construction, operation and testing are included in section **Error! Reference source not found.**. Reflections from M1 and M2 respectively form the measurement and reference beams of the IFPI and follow a common-mode path back through the fibre switch and FOC to the interrogation interferometer.

Within the interrogation interferometer, the light from the strain gauge is collimated into free space and split into the two arms of an unbalanced Michelson interferometer. The mismatched Michelson interferometer arms of length a_1 and a_2 serve to bring the light from M1 and M2 back into coherence by reflection from M3 and M4. The shorter path length in the interferometer arm (a_2) accounts for the longer distance travelled by the light reflected from mirror M2 and the short coherence of the source light. The phase difference per unit length, f{k}, for light of wavenumber k can be described as follows:

$$\theta\{k\} = 2ka_1 - 2(ka_2 + f\{k\}d) \qquad (1)$$

Light reflected from M3 and M4 is then recombined at the beam splitter (BS) before being spectrally decomposed by a spectrometer comprising a reflective grating (G3), a spherical mirror (SM) and a CMOS linear array (D)(Basler Racer raL8192). This provides measurement of strain at a single channel rate of 6 kHz, limited by the detector. The resulting spectral interferogram, I{k}, can be described as follows:

$$I\{k\} = B\{k\} + A\{k\}cos(\theta\{k\}) \qquad (2)$$

Where $B\{k\}$ is a non-interfering D.C. component from non-coherent light paths and $A\{k\}$ is the amplitude of the sinusoidal interferogram, an example of which is illustrated as the grey plot in figure 4.

As strain is applied to the fibre strain gauge length, d, the small change in optical path length, δd, results in a shift in the interferogram frequency. The path length change and

hence strain is obtained by calculating the phase slope of the unwrapped instantaneous phase of the interferogram [8]. In previous bench test work (unpublished), we have demonstrated a strain resolution of 0.1 με and a range of 80 με.

2.2 Fibre probes

The strain sensitive IFPI cavities are assembled by bonding 160 mm of 780HP single-mode fibre into an LC/PC ferrule. After polishing of the LC/PC ferrule, the assembly is inserted into a jig and the bare fibre end cleaved to provide an IFPI of length 150 mm ± 10 µm. Next, a titanium oxide/silicon dioxide (Ti_3O_5/Sio_2) coating is applied to each end of the IFPI cavity with a 30% reflection coating on the LC/PC ferrule end and a 100% coating on the bare fibre end. This serves to increase the power of the reflected light hence increasing the robustness of the system to fibre darkening and allowing an increase of the measuring rate. The sinusoidal signal from the IFPI cavities before (grey) and after coating (orange) is shown in figure 3.

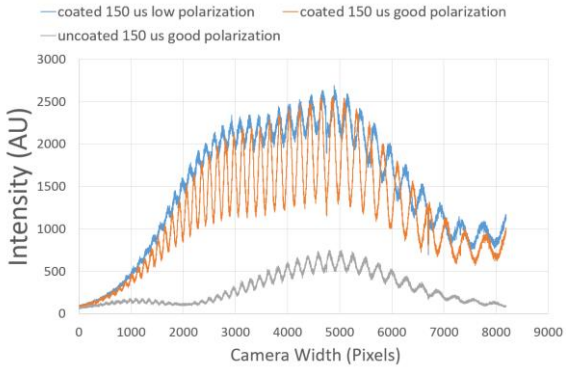

Figure 3. Signal response from IFPI cavity before (grey) and after coating (orange)

The blue trace illustrates the effect of polarisation adjustment on eth amplitude. Adjustment is built into the fibre routing to maximum amplitude for all fibres. As can be seen the resultant signal intensity has increased by nearly 400%. Lastly, the LC/PC ferrule is mechanically mated with a bare fibre patch cable using a split ceramic ferrule and the whole assembly is clamped to the collimator jaws.

Figure 4. IFPI cavities bonded to scale model of jaw

Shown in figure 5 are examples of the IFPI cavities bonded to a scale model of the ACS collimator jaw.

3. Integration

3.1 Placement

For monitoring of jaw displacement, each jaw encompasses twelve IFPI cavities arranged into two tracks of six running the full length of the jaw. Limited by the design of the ACS jaw, the two lines of sensors are placed with as much separation as possible. This allows for the maximum amount of differentiation between probes corresponding in the front and back tracks. Figure 5 shows the track placement with respect to the overall jaw design.

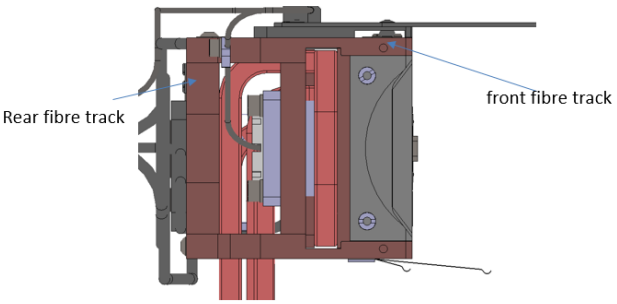

Figure 5. End view of the ACS jaw showing fibre track placement

This configuration will allow for jaw displacement direction and magnitude to be deduced from the differentiation between the strain values of corresponding probes on the front and back tracks.

3.2 *Temperature and radiation hard fibres*

For this system to work within the harsh environment of the LHC, the standard 780HP fibres are being replaced with a high temperature resistant, pure silica core version.

Whilst the operating temperature of the collimator is not a primary concern, to achieve the ultra-high vacuum levels required of the LHC, the collimators are baked to 250 °C for 48 hours before being installed. One of the reasons for this choice of fibre is that this 780HP copper variant has a long-term maximum temperature rating of 450 °C.

In addition to this, utilizing a pure silica core maximises the fibres' longevity by minimising its susceptibility to radiation darkening. Even at low levels, presence of Germanium dioxide dopants in the fibre core makes the optical fibre susceptible to darkening and increased attenuation [9].

A sample of the pure silica core fibre was placed in an 8 MeV linear accelerator along with two samples of the standard 780HP fibre. The samples were place 7 m away from the source of the accelerator and kept there for nine months, receiving an average weekly dose of 117 Gr of ionizing radiation. Periodically the samples were connected to a SLED and a power meter; with the level of power transmission recorded. Figure 6 shows the results of this test.

The results show that whilst the standard 780HP fibres do show signs of recovery, overall power transmission decreases over time. However, the pure silica version shows no attenuation, generally maintaining its power transmission over the entire timeframe. The differing levels of power intensity between the three plots is due to the lack of polarization control within the set up.

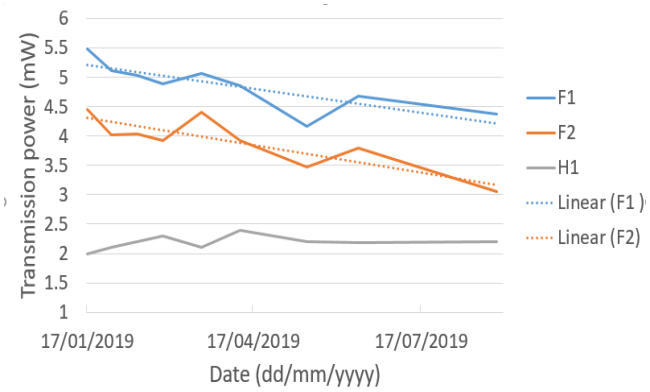

Figure 6. Fibre Transmission results

4. Preliminary Benchmarking

As shown in figure 4 several IFPI probes were bonded to a scale model of the jaw. The jaw was then oscillated at 3 Hz and its response recorded by both the IFPI probes and a Renshaw XL-80. Figure 7 shows the first order response captured by the XL-80 and the second order response recorded by a single IFPI probe.

The above results show that the IFPI probes are capable of recording a first order micron displacement from a second order orientation. The discrepancies in magnitude are also due to this orientation. If the data shown were a differentiation between two corresponding probes, at the front and the back of the jaw, the magnitude values would be comparable. This is to be validated in upcoming work.

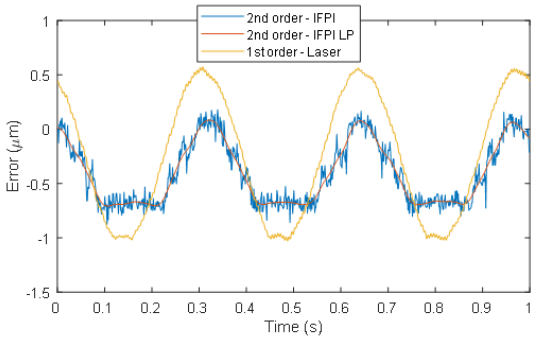

Figure 7. First and second order dynamic displacement comparison

5. Conclusions and Future work

The Spectral Interferometry fibre strain measurement system has provided a viable solution for the measurement of transverse deformation in collimator jaws. Additional work on aspects of integration give the system a higher chance of longevity whilst operating inside the LHC environment.

Initial observations indicate that the system is sensitive enough to observe a second order response from a 1.5 µm first order displacement.

Several areas however have been identified that would further optimised the system in this context and will warrant further investigation.

The current optical system uses TDM to interrogate multiple fibre strain gauges. Future work will investigate the use of varying length sensors and spatial frequency division multiplexing (SFDM) [10] to interrogate all 8 strain gauges simultaneously. This will eliminate the measurement rate reduction introduced when using a fibre switch to time division multiplex the signals.

To lower the sensor cost and ease installation we will investigate manufacture of in-line reflectors by methods such as fibre splicing of coated fibres [11].

One additional advantage of using copper clad fibres is the potential to weld them to the metallic structure of the jaw. Research [12] has shown that with a sufficient diameter metal cladding the fibres can be TIG welded to the part under scrutiny. This has been attempted with the current fibres being used with limited success due to the small diameter cladding.

Finally, once the ACS prototype is fully assembled, and primary validation has been performed, the prototype and the measurement system will be relocated to CERN for final validation under beam conditions.

Acknowledgments

The authors would like to thanks The European Council for Nuclear Research (CERN), and the UK's Science and Technologies Facilities Council (STFC), who have funded this project as part of the HL-LHC upgrade, grant No. ST/N001699/1.

References

[1] Tygier, S., Appleby, R., et al. "*Recent development and results with the merlin tracking code",* in Proc. International Particle Accelerator conference (IPAC2017), Copenhagen, Denmark, 2017, MOPAB013, pp 104-106

[2] Arduini, G., et al. *"High Luminosity LHC: Challenges and Plans",* in Proc. 14th Topical Seminar on Innovative Particle and Radiation Damage (IPRD'16), Siena, Italy, Dec 2016, doi: 10.1088/1748-0221/11/12/C12081

[3] Furness, T., et al. "*Adaptive Collimator Design for Future Particle Accelerators",* in Proc. 7th International Beam Instrumentation Confernce (IBIC '18), Shanghai, China, 2018,doi:10.18429/JACoW-IBIC2018-TUPA15

[4] Bertarelli, A,. et al. "*The mechanical design for the LHC Collimators"*, in Proc. 9th European Particle Accelerator Confernce (EPAC '04), Lucerne, Switzerland, Jul 2004, MOPLT010, pp 545-547

[5] Carra, F., "*Thermomechanical Response of Advanced Materials under Quasi-Instantaneous Heating",* Ph.D. thesis, Politecnico di Torino, Italy, 2017.

[6] Mereghetti, A., *et al*., "*BLM Thresholds and Damage Limits for Collimators*", in *Proc. 6th Evian Workshop on LHC Beam Operations,* Evian les Bains, France, Dec 2015, pp 197-202.

[7] Potdar, A., et al., *"Performance characterisation of a new photo-microsensor based sensing head for displacement measurement",* in Sensors and Actuators A: Physical, Vol 238, 2016, Elsevier, pp 60-70

[8] Takeda, M., Mutoh, K., "*Fourier transform profilometry for the automatic measurement of 3-D object shapes*", in Applied optics, Vol 22(24), 1983, pp 3977-3982

[9] Girard, S., et al., "*Overview of radiation induced point defects in silica-based optical fibres",* in Reviews in Physics, Vol 4, 2019, Elsevier

[10] Rao, Y. J., et al., "*Demodulation algorithm for spatial-frequency-division-multiplexed fiber-optic Fizeau strain sensor networks*", in Optics letters, Vol 31(6), 2006, pp 700-702.

[11] Cibula, E., Donlagic, D., "*Low-loss semi-reflective in-fiber mirrors*", in Optics express, Vol 18(11), 2010, pp 12017-12026.

[12] Grandel, T., et al., "*analysis of fibre optics sensor embedded in metals by automatic and manual TIG welding*", in IEEE Sensors Journal, Vol.19, 2019, IEEE, pp 7425-7432